AN AIRCRAFT STUDY OF TURBULENCE DISSIPATION RATE AND TEMPERATURE STRUCTURE FUNCTION IN THE UNSTABLE MARINE ATMOSPHERIC BOUNDARY LAYER

C. W. FAIRALL

BDM Corporation, Naval Postgraduate School, Monterey, California 93940, U.S.A.

RALPH MARKSON

Airborne Research Associates, 46 Kendal Common Road, Weston, Massachusetts 02193, U.S.A.

G. E. SCHACHER and K. L. DAVIDSON

Environmental Physics Group, Naval Postgraduate School, Monterey, California 93940, U.S.A.

(Received in final form 27 March, 1980)

Abstract. The dissipation rate of turbulent kinetic energy, ε, and the temperature structure function parameter, C_T^2, have been measured over water from the near surface ($Z = 3$ m) to the top of the boundary layer. The near surface values of ε and C_T^2 were used to calculate the velocity and temperature Monin–Obukhov scaling parameters u_* and T_*. The data collected during unstable lapse rates were used to evaluate the feasibility of extrapolating the values of ε and C_T^2 as a function of height with empirical scaling formulae. The dissipation rate scaling formula of Wyngaard *et al.* (1971a) gave a good fit to an average of the ε data for $Z < 0.8\ Z_i$. In the surface layer the scaling formula of Wyngaard *et al.* (1971b) disagreed with the C_T^2 values by as much as 50%. This disagreement is due to an unexpected reduction in the measured values of C_T^2 for $Z < 30$ m. At this point it is not clear if the discrepancy is a unique property of the marine boundary layer or if it is simply some unknown instrumental or analytical problem. The mixed layer scaling results were similar to the overland results of Kaimal *et al.* (1976).

1. Introduction

This paper is a report on measurements of temperature structure parameter, C_T^2, and rate of dissipation of turbulent kinetic energy, ε, made from a light aircraft using microthermal sensors as part of a study of turbulence in the marine boundary layer. A typical flight included measurements as low as 3 m above the sea surface in an effort to characterize surface-layer turbulence parameters. The flights were usually extended well above the inversion – a maximum altitude of 3 km being typical. The data were gathered near Panama City, Florida as part of a program of marine boundary-layer research, the ultimate goal of which is the formulation of a model that will allow reasonable estimates of atmospheric turbulence and mean properties from the surface throughout the entire marine boundary layer and immediately above. Such a model would have application to such varied subjects as turbulent transport of heat, water vapor and pollutants, optical propagation, aerosols, radar propagation and communications.

This paper will focus on the utilization of the data to examine certain aspects of the Monin–Obukhov similarity (MOS) expressions for the dimensionless temperature structure function and the dimensionless dissipation function in the marine atmos-

Boundary-Layer Meteorology **19** (1980) 453–469. 0006–8314/80/0194–0453$02.55.

pheric boundary layer. The validity of existing empirical expressions of asymptotic height dependencies, variance of the data from surface extrapolations and the influence of the height of the boundary layer will be explored. Of the nine days on which flights were made, seven were characterized by unstable surface layers and two by stable surface layers. Since the height of the boundary layer was so low on the *stable* days (typically 100 m), the influence of the height of the boundary layer tended to dominate surface-layer conditions causing most of the quantitative analyses mentioned immediately above to be of dubious relevance. In view of this, the analysis of surface-layer scaling properties was restricted to unstable cases.

2. Theoretical Background

Kaimal *et al.* (1976) divide the unstable boundary layer into three regions: the surface layer (Monin–Obukhov scaling), the free convection layer and the mixed layer. Panofsky (1977) points out that the free convection layer is a region where Monin–Obukhov scaling and mixed layer scaling both apply; hence he has called this region the convective matching layer defined by $-L < Z < 0.1\, Z_i$.

In the surface layer the scaling parameters for velocity, temperature and water vapor (u_*, T_*, and q_*) are defined (those interested in a more complete treatment should refer to Businger, 1973 and Wyngaard *et al.*, 1971a and 1971b)

$$\tau_0 = \rho u_*^2 \tag{1a}$$

$$Q_0 = -u_* T_* \tag{1b}$$

$$M_0 = -u_* q_* \tag{1c}$$

where ρ is the density of air and τ_0, Q_0, M_0 are the fluxes of momentum, sensible heat and water vapor, respectively.

The Monin–Obukhov length, L, is defined as

$$L = -Tu_*^3/\kappa g Q_{0V} \tag{2}$$

where $\kappa = 0.35$ is von Kármán's constant, g is the acceleration of gravity, T the absolute temperature and Q_{0V} is the virtual temperature flux equal to $Q_0 + (0.61\, TM_0/\rho)$.

In the surface layer, one can write expressions for ε and C_T^2

$$\varepsilon = (u_*^3/\kappa Z)\phi_\varepsilon(\xi) \tag{3a}$$

$$C_T^2 = T_*^2 Z^{-2/3} f(\xi) \tag{3b}$$

where $\xi = Z/L$. The present form of the dimensionless dissipation function, $\phi_\varepsilon(\xi)$, is (Wyngaard *et al.*, 1971a).

$$\phi_\varepsilon(\xi) = (1 + 0.5|\xi|^{2/3})^{3/2} \qquad \xi < 0 \tag{4a}$$

$$\phi_\varepsilon(\xi) = (1 + 2.5|\xi|^{2/3})^{3/2} \qquad \xi > 0 \tag{4b}$$

while that for the dimensionless structure functions parameter, $f(\xi)$, is (Wyngaard *et al.*, 1971b)

$$f(\xi) = 4.9(1 - 7\xi)^{-2/3} \qquad \xi < 0 \tag{5a}$$

$$f(\xi) = 4.9(1 + 2.4\xi^{2/3}) \qquad \xi > 0. \tag{5b}$$

The appropriate velocity and temperature scaling quantities for the mixed layer are (Kaimal *et al.*, 1976)

$$\omega_* = [(g/T)Q_{0v}Z_i]^{1/3} \tag{6a}$$

$$\theta_* = Q_0/\omega_* \tag{6b}$$

where Z_i is the height of inversion. In the convective matching region, the mixed-layer scaling of the turbulent quantities gives

$$\varepsilon Z_i/\omega_*^3 \to A \tag{7a}$$

$$C_T^2 Z_i^{2/3}/\theta_*^2 \to B(Z/Z_i)^{-4/3} \tag{7b}$$

where A and B are constants. Kaimal *et al.* (1976) found that Equation 7 applies not only in the convective matching layer but well into the mixed layer.

3. Instrumentation and Analysis

The platform for these measurements is a single engine turbo-charged Bellanca Viking operated by Airborne Research Associates. The aircraft is also equipped to allow simultaneous instrumental measurements of air temperature, pressure, dew point, electric field, and infrared surface temperature. Details of the instrumentation and data acquisition are contained in a technical report (Fairall and Markson, 1979). We will only discuss certain aspects of the turbulence measurements deemed relevant to the interpretation of the data.

Dissipation rate, ε, was determined from velocity fluctuations sensed with a constant temperature anemometer employing tungsten wires 4.5 μm in diameter and 1.7 mm in length operated at a 50% overheat. The signal was bandpass filtered (f_l = 50 Hz and f_u = 500 Hz) before being squared and averaged. One can calculate ε from the *filtered* mean square fluctuations using

$$\varepsilon^{2/3} = \left(\frac{2\pi}{\bar{u}}\right)^{2/3} \frac{2}{3(0.52)} \frac{\langle (u - \bar{u})^2 \rangle_{l,u}}{(f_l^{-2/3} - f_u^{-2/3})} \tag{8}$$

where $\bar{u}$ = 60 m s^{-1} is the average aircraft true airspeed (with the assumption that f_l and f_u are within the inertial subrange).

Temperature structure function, C_T^2, was determined from temperature difference fluctuations sensed with paired tungsten wires separated a distance d = 0.85 m. Two complete systems were used (one a.c. Wheatstone's bridge and one d.c.) each employing an independent pair of wires. The frequency response of the sensors and bridges were approximately 800 Hz. The two systems systematically disagreed by

about 20%, probably due to inaccurate calibration of the d.c. bridge. The *velocity* sensitivity of the sensors as a function of bridge current was carefully measured at $\bar{u} = 60$ m s^{-1} in the laboratory to optimize the temperature fluctuation measurements. The mean-square temperature fluctuation data were corrected for velocity effects using the known velocity sensitivity and the values of velocity fluctuation intensity measured simultaneously with the hot-wire anemometer. Furthermore, one temperature bridge was operated at half the sensor current of the other in order to flag possible velocity sensitivity problems, should they occur. In practice, the velocity contribution to the temperature signal was considerably less than the system noise. C_T^2 was calculated using the equation

$$C_T^2 = \langle (T(x) - T(x + d))^2 \rangle_d d^{-2/3} \tag{9}$$

which is based on the assumption that the probe separation, d, is within the inertial subrange.

Because the larger scale eddies are under the boundary influence as one approaches the sea surface, the measured values of C_T^2 and ε are subject to error due to the assumptions of isotropy in Equations 8 and 9. This is particularly important for these data because of the unusually low altitudes ($Z \approx 3$ m) employed. We have examined this question by replacing the inertial subrange forms of S_u and S_T with forms valid over the entire range of k. Thus, we can compute the actual *measured* values of the mean square fluctuations

$$\langle (u - \bar{u})^2 \rangle_{l,u} = \int_{f_l}^{f_u} S_u(f)\, \mathrm{d}f \tag{10a}$$

$$\langle (T - \bar{T})^2 \rangle_d = 2 \int_0^{\infty} [1 - \cos(dk)] S_T(k)\, \mathrm{d}k \tag{10b}$$

where we have used the formulae for S_u and S_T given by Kaimal *et al.* (1972) for *neutral* stability. Since Kaimal *et al.* (1972) indicate that the size scales for unstable conditions are considerably larger than the neutral case, this calculation should serve to establish an upper limit on the effects. We have expressed the result in terms of the calculated ratio of the measured to the actual value ($\varepsilon_m/\varepsilon$ or C_{Tm}^2/C_T^2) as a function of altitude (Figure 1a) for filter frequencies and probe spacing used in the experiment. Based on this calculation, one can conclude that the isotropy effects on the measurements of ε were negligible and that the upper limit of the effects on the C_T^2 were on the order of 10%. This conclusion was tested by making simultaneous C_T^2 measurements with two pairs of sensors spaced at $d = 0.85$ m (d.c. bridge) and $d = 0.30$ (a.c. bridge). The ratio of these C_T^2 measurements is given in Fig. 1b. Violation of the isotropic turbulence assumption would show up as a decrease of this ratio as one approaches the surface. The fact that the ratio actually increases (although this small increase is of marginal significance) suggests that some other phenomenon is influenc-

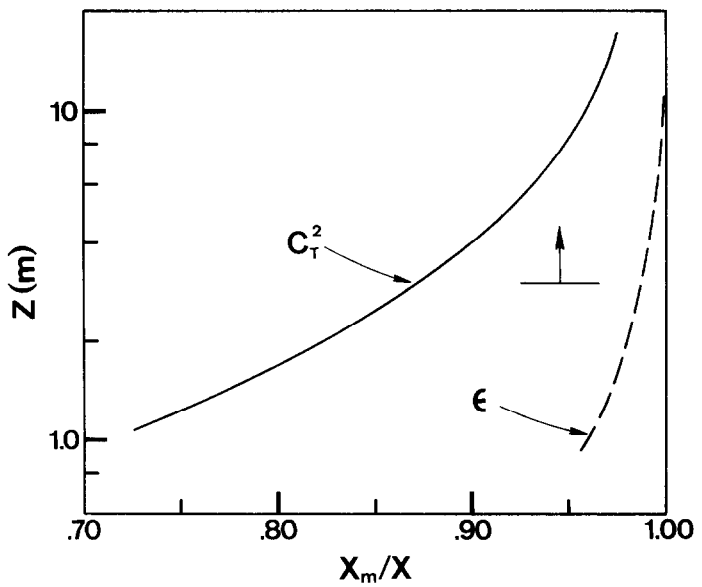

Fig. 1a. The expected effect of the lower isotropic limit on the turbulence measurements as the aircraft nears the sea surface. The measurement error is expressed as the ratio of the measured value to the actual value (X_m/X) for ε (dashed line) and C_T^2 (solid line) from calculations using Equations 10a and 10b. Empirical expressions for the turbulence spectra were taken from Kaimal *et al.* (1972) for neutral stability and are intended to yield an estimate of the upper limit of the effect. The short horizontal line with the vertical arrow indicates the minimum altitude of the aircraft.

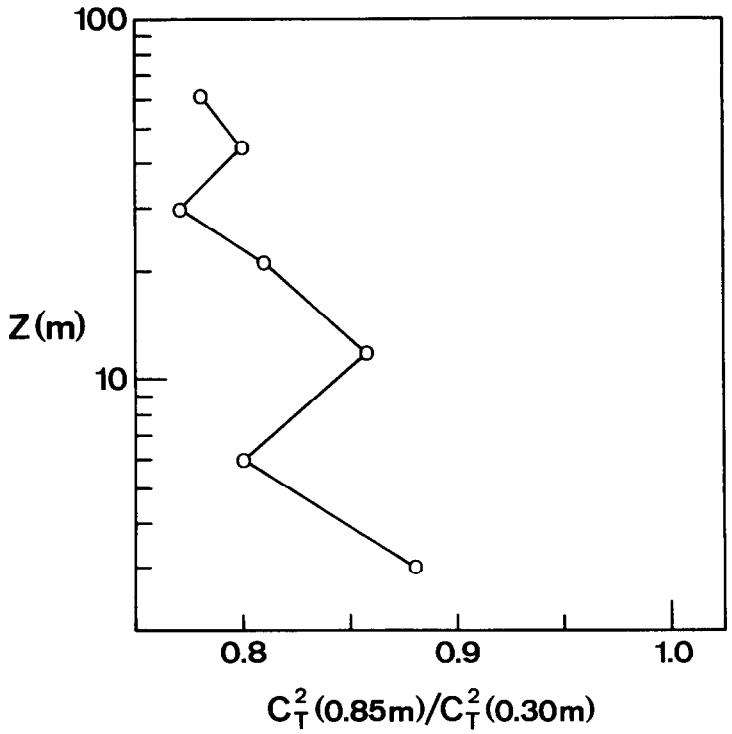

Fig. 1b. Ratio of C_T^2 as measured with $d = 0.85$ m to that measured with $d = 0.30$ m as a function of altitude. Each point represents the average of two 4-min. level runs.

ing the C_T^2 measurements near the surface. The influence of this effect is discussed later.

4. Flight Pattern

Aircraft are particularly useful for atmospheric research because they are able to sample large volumes of atmosphere in relatively short time periods. Unfortunately, even at 60 m s^{-1}, one cannot expect to tranverse the larger scale eddies normally associated with turbulence in just a few seconds. As a result, if one wishes to define the turbulence properties of the atmosphere with some reasonable statistical confidence, an averaging period of a few minutes (on the order of 10 km))is required. Obviously for the surface layer investigation, one not only requires very low altitude data but a greater density of measurement altitudes near the surface. The final choice of flight pattern consisted of a series of constant altitude runs of 2-min duration each at successively greater altitude. In order to maintain the same approximate location, the flight direction was reversed at alternative altitudes. Normally the process was started at the lowest altitude of 3 m, as 'eyeball' estimated by the pilot. At this point the aircraft altimeter was set to 3 m and subsequent altitudes were based on this setting. The altitudes of the level runs were increased approximately exponentially.

This type of flight pattern has been named a 'ladder profile' with the 2-min runs being the rungs of the ladder. The total time required to execute a complete ladder profile was on the order of 30 min.

5. Surface-Layer Scaling Parameters

The Monin–Obukhov scaling parameters for each profile were obtained from the lowest two or three data points. First, q_* was calculated from a simple bulk formulation using a 10 m drag coefficient

$$q_* = 0.036(q - q_s) \tag{11}$$

where q is the mixing ratio at $Z = 10$ m and q_s is the value for the sea surface calculated from the sea surface temperature assuming 100% relative humidity. Given the relatively smaller contribution of q_* to L, a more sophisticated treatment of water vapor was not considered to be worthwhile. At this point, values of u_* and T_* were selected that gave good fits of Equations 3a and 3b to the lower altitude values of ε and C_T^2. Since $|\xi|$ was usually much less than unity in this region, the actual form of $\phi_\varepsilon(\xi)$ and $f(\xi)$ would be de-emphasized in the determination of u_*, T_* and L. The sign of T_* was determined from the air–sea temperature difference. The scaling parameters for all 21 profiles taken are given in Table I.

TABLE I

Surface-layer scaling parameters for the ladder profiles obtained. N is the number of points in each profile; the other quantities are defined in the text

Profile No.	Date	Time	u_* (m s^{-1})	T_* (°C)	q_* (gm kg^{-1})	L (m)	Z_i (m)	N
1	11/26	1252	0.40	−0.082	−0.160	−125	850	14
2	11/26	1436	0.23	−0.095	−0.160	− 50	900	14
3	12/02	1405	0.24	−0.135	−0.180	− 29	230	18
4	12/03	1108	0.29	0.030	0.000	233	200	11
5	12/03	1201	0.24	0.015	−0.018	420	60	10
6	12/03	1232	0.18	0.024	−0.009	120	60	9
7	12/03	1339	0.34	0.031	−0.040	403	120	11
8	12/05	1532	0.24	−0.260	−0.410	− 15	700	10
9	12/05	1624	0.36	−0.270	−0.400	− 16	700	13
10	12/07	1511	0.25	0.015	−0.007	390	75	12
11	12/07	1601	0.23	0.025	0.010	171	100	11
12	12/10	1259	0.53	−0.440	0.000	− 53	760	10
13	12/10	1324	0.38	−0.350	0.000	− 34	760	11
14	12/10	1410	0.32	−0.490	−0.490	− 15	760	15
15	12/10	1523	0.34	−0.480	−0.470	− 17	820	14
16	12/10	1637	0.34	−0.490	−0.500	− 16	980	14
17	12/11	1021	0.28	−0.440	−0.430	− 13	700	12
18	12/12	1642	0.28	−0.180	−0.500	− 24	800	18
19	12/13	1154	0.19	−0.210	−0.470	− 10	600	17
20	12/13	1459	0.17	−0.200	−0.420	− 9	550	14
21	12/13	1721	0.14	−0.120	−0.440	− 5	450	17

6. Ladder Profiles

The locations of the profiles are indicated in Fig. 2 by profile number. Overland profiles, 12 and 13, were not used in the results presented later. Since the profile data are completely catalogued elsewhere (Fairall and Markson, 1979), we will give only a few examples here. The situation encountered for the stable surface layers is illustrated in Fig. 3 where the deviations of C_T^2 from the surface-layer expression (Equation 3b) extend down to the lowest altitudes. The example given is one of the extremes; there were other stable profiles where the fit was much better, but, in general, the stable surface layers appeared to be dominated by the shallowness of the boundary layer.

The boundary layer was much more extensive on unstable days (the inversion height was typically 800 m). In profile No. 1 (Fig. 4a) the surface layer expression for C_T^2 is a good fit up to at least 300 m. Note that in this case the upper altitude values of ε are smaller than expected based on the near surface values, while in profile No. 19 (Fig. 4b) the reverse is true. This effect may be due to the fact that we ignored the possible existence of wind roll vortices (LeMone, 1973) or other two-dimensional structure. In Fig. 4b the C_T^2 data display a feature that often occurred. The higher altitude values are well fit by a $Z^{-4/3}$ curve but the actual values are not consistent

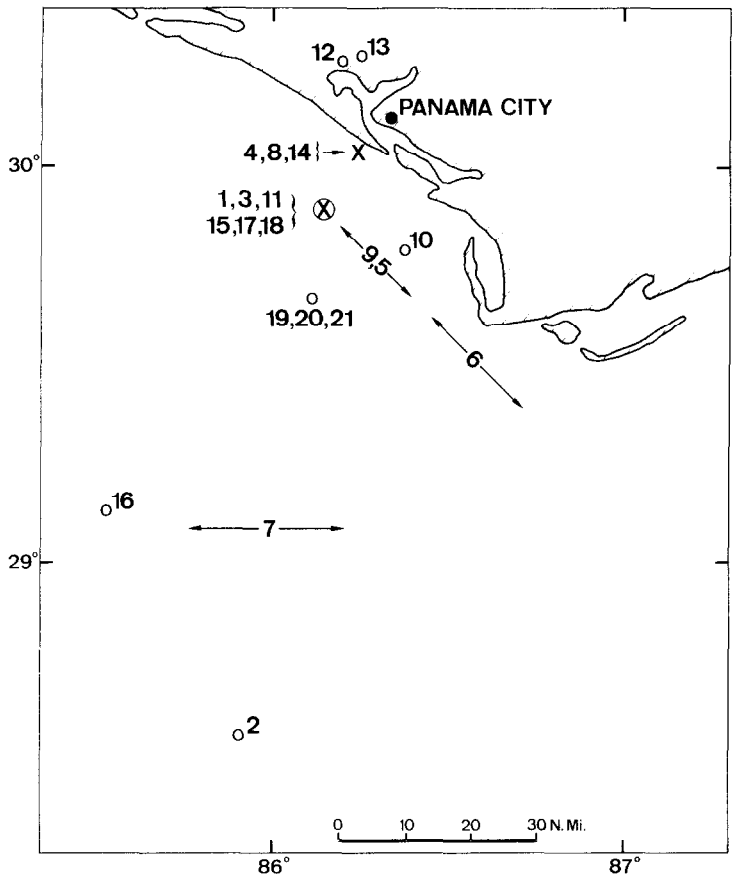

Fig. 2. Locations of the ladder profiles in the vicinity of Panama City, Florida. The ⊗ and × represent offshore platforms known as Stage I and Stage II, respectively. The numbers are the corresponding ladder profile designations.

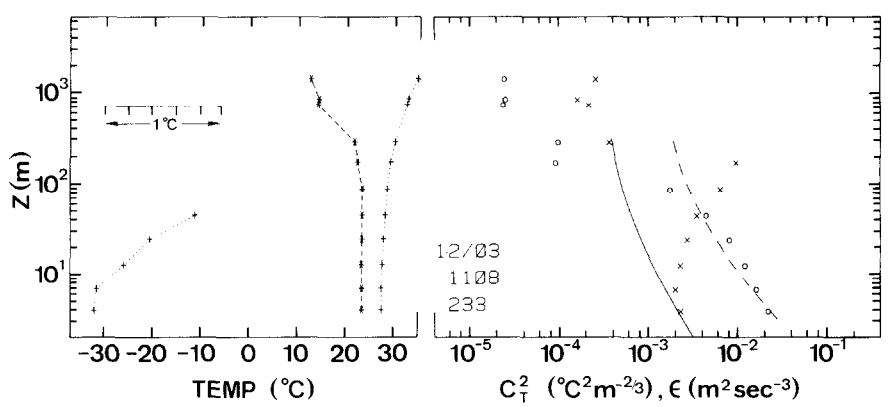

Fig. 3. Ladder profile No. 4. The data points plotted are virtual potential temperature (+), dew point temperature (*), C_T^2 (×) and ε (○). The solid line is the MOS expression for C_T^2 and the long-dash line is the MOS expression for ε. The extreme left-hand side of the graph shows an expanded scale plot of virtual potential temperature. The date, time and Monin–Obukhov stability length, L, are given in the lower center of the graph.

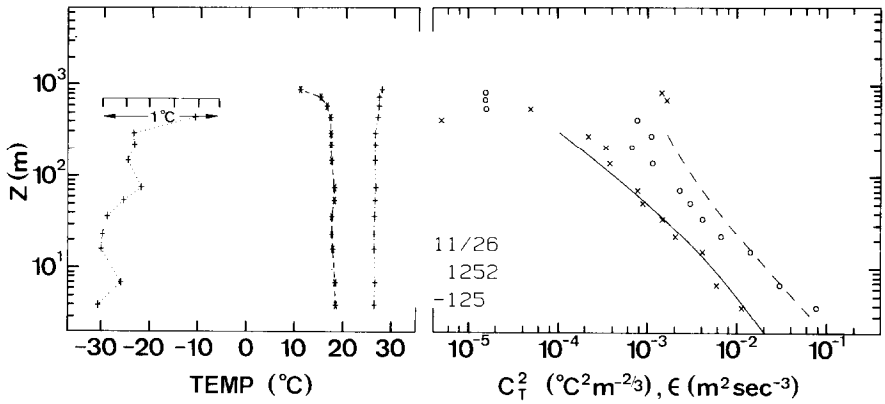

Fig. 4a. Ladder profile No. 1. The data points plotted are virtual potential temperature (+), dew point temperature (*), C_T^2 (×) and ε(○). The solid line is the MOS expression for C_T^2 and the long-dash line is the MOS expression for ε. The extreme left-hand side of the graph shows an expanded scale plot of virtual potential temperature. The date, time and Monin–Obukhov stability length, L, are given in the lower center of the graph.

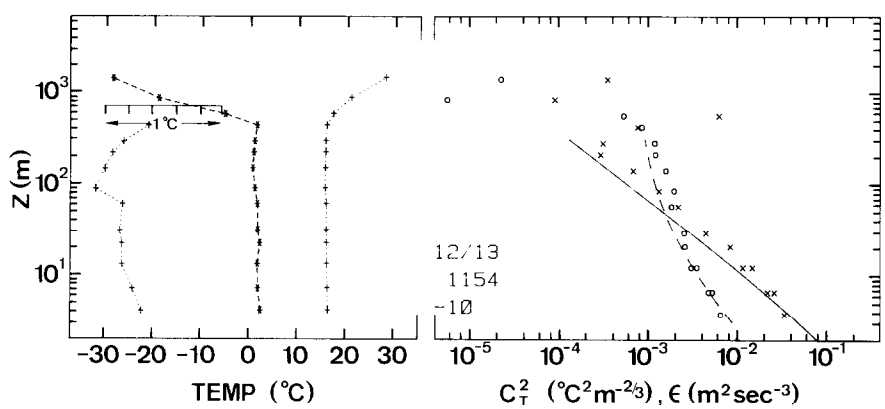

Fig. 4b. Ladder profile No. 19. The data points plotted are virtual potential temperature (+), dew point temperature (*), C_T^2 (×) and ε (○). The solid line is the MOS expression for C_T^2 and the long-dash line is the MOS expression for ε. The extreme left-hand side of the graph shows an expanded scale plot of virtual potential temperature. The date, time and Monin–Obukhov stability length, L, are given in the lower center of the graph.

with the near surface values, which were somewhat lower than expected on the basis of the $Z^{-4/3}$ region. This aspect will be discussed in Section 9.

7. Surface-Layer Scaling Results

Given values of u_* and T_* for an unstable profile, the dimensionless quantities $\varepsilon\kappa Z/u_*^3$ and $C_T^2 Z^{2/3}/(4.9\ T_*^2)$ were calculated for each data point. Because u_* and T_* were determined from the near-surface values of ε and C_T^2, the dimensionless quantities automatically have values near unity for $-Z/L \ll 1$. The dimensionless values were

then averaged in bins of different dimensionless stability length allocated according to $\log|Z/L|$. Since the number of profiles taken on a given flight varied from one to five, a weighted average was used to avoid overemphasizing conditions during flights with more profiles. Each profile was assigned a weight $W = 1/M$ where M was the number of overwater profiles in that flight. In order to eliminate effects due to the inversion, the data had to be restricted based upon Z_i. The criteria that allowed the most data to be used without introducing inversion effects were

$$Z < 0.8\, Z_i \qquad \text{for } \varepsilon \tag{12a}$$

$$Z < 0.4\, Z_i \qquad \text{for } C_T^2. \tag{12b}$$

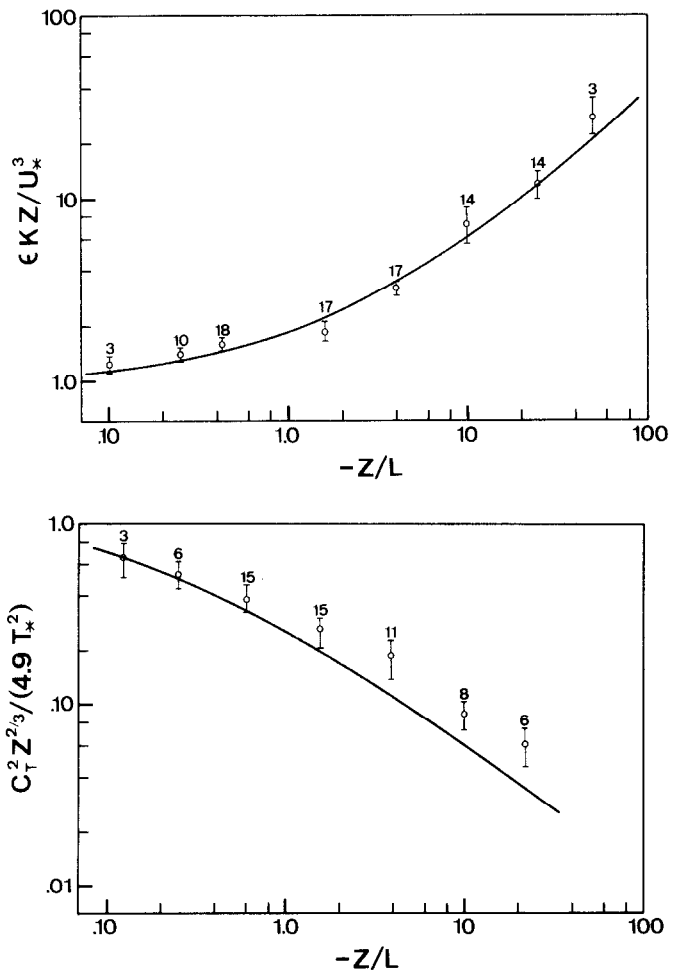

Fig. 5. Dimensionless turbulence measurements as a function of dimensionless atmospheric stability. The points represent the weighted average of the profile data, the vertical bars represent the statistical error in the mean estimate and the number is the weighted number of points in the average. (a) Dimensionless dissipation rate for $Z < 0.8\, Z_i$. The solid line is from Equation 4a. (b) Dimensionless temperature structure function for $Z < 0.4\, Z_i$. The solid line is from Equation 5a.

The results are given in Fig. 5a and 5b, the solid curves representing Equation 4a and Equation 5a, respectively.

In order to examine the absolute height dependence (rather than the scaled height dependence), a quantity R was calculated for each data point where R is the ratio of the dimensionless turbulence value to that value one would expect based on Equations 4a and 5a.

$$R_\varepsilon = (\varepsilon k Z/u_*^3)(1 + 0.5|Z/L|^{2/3})^{-3/2} \tag{13a}$$

$$R_T = (C_T^2 Z^{2/3}/4.9\, T_*^2)(1 - 7\, Z/L)^{2/3}. \tag{13b}$$

The values of R were then averaged in bins of different altitude in a manner similar to that just described. The averages of R are shown in Fig. 6 and the ratio of the standard deviation, σ_R, to R is shown in Fig. 7. Taken together, these two figures illustrate one's ability to predict ε and C_T^2 as a function of height from near-surface measurements. The 20% standard deviation for the near-surface values (Fig. 7) is due to the scatter inherent in the 2-min averages.

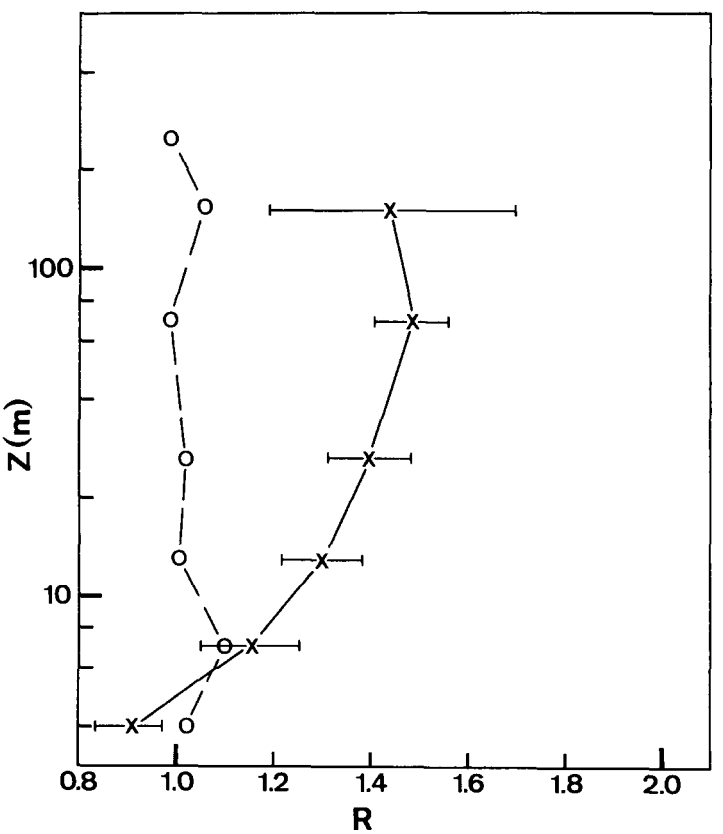

Fig. 6. Weighted average of R *vs* altitude where R is the ratio of the measured value of the turbulence quantity to that value expected from Equation 3a or Equation 3b. The circles are for ε and the $\times$'s are for C_T^2. The horizontal bars represent the errors in the mean estimate (the errors for C_T^2 and ε were similar).

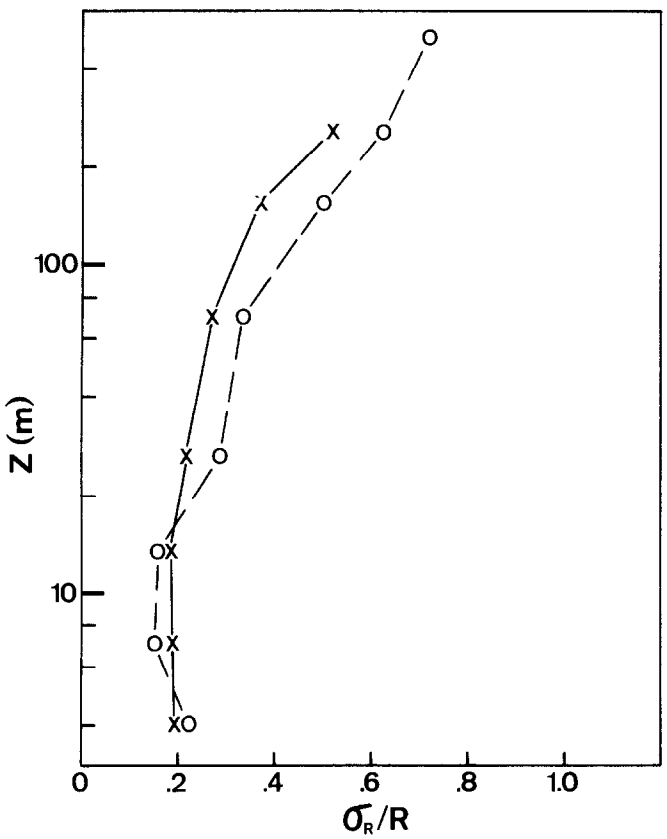

Fig. 7. Fractional random error in predictions of turbulence profiles form near surface measurements using Equation 4a and Equation 5a. The circles are for ε and the $\times$'s are for C_T^2. The near surface value of $\sigma_R/R = 0.2$ is due to the measurement scatter of the two-minute averages.

8. Mixed-Layer Scaling Results

The average profiles of virtual potential temperature and water vapor mixing ratio are shown in Fig. 8 (see Wyngaard *et al.*, 1978, for comparison). In order to compare with the over-land results of Kaimal *et al.* (1976), we have plotted the turbulence data (Fig. 9) in the dimensionless forms

$$\varepsilon/\frac{g}{T}Q_{0v} \rightarrow A \tag{14a}$$

$$C_T^2/3.2\,\theta_*^2 Z_i^{-2/3} \rightarrow B(Z/Z_i)^{-4/3}. \tag{14b}$$

The convective limit of Equation 4a gives $A = 0.36$. Lenschow (1974) has found $A = 0.43$ while Kaimal *et al.* (1976) measured values of A between 0.5 and 0.7 over-land. Actually, an asymptotic limit was reached only on profile 21 which happened to be more consistent with $A = 0.5$.

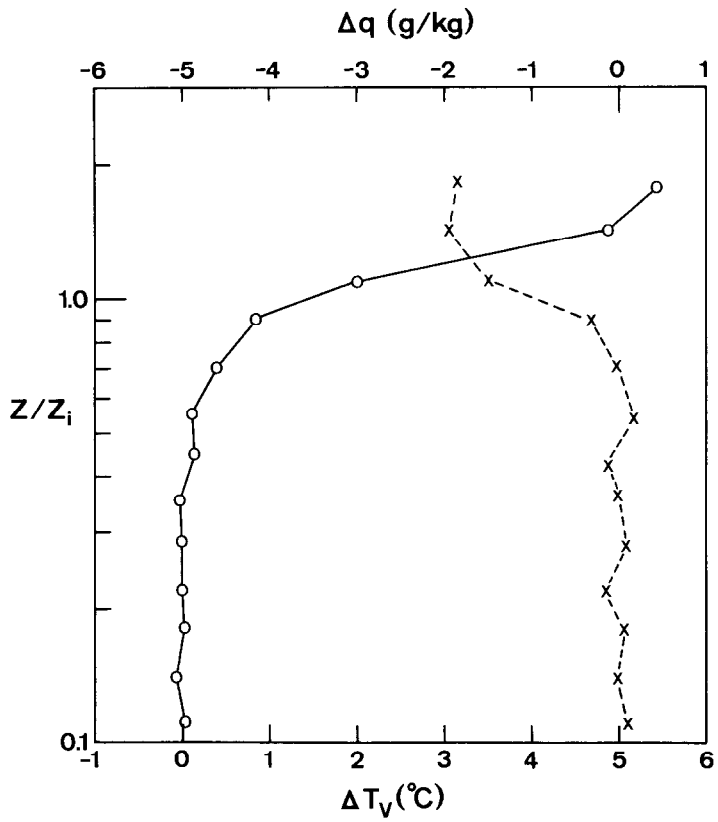

Fig. 8. Average profile of virtual potential temperature (circles, $\overline{T_v} = 17.0\,^{\circ}\mathrm{C}$) and water vapor mixing ratio ($\times$'s, $\bar{q} = 6.1$ g kg^{-1}) for the Panama City unstable data. The data are plotted as $\Delta x = x - \bar{x}$ where $\bar{x}$ is taken at $Z = 0.1\ Z_i$.

The convective limit of Equation 5b gives B = 0.83 which agrees with the mixed-layer value obtained by Kaimal *et al.* (1976). The solid line in Fig. 9b is a representation the results of Kaimal *et al.* (1976) with $B = 1.30$. The mixed-layer turbulence results can be viewed in a different perspective by plotting the quantity R (Equation 13) as a function of Z/Z_i (Fig. 10). A value of 1.0 for the ratio would indicate agreement between the surface-layer scaling parameters and equations (Equation 3) with the lower mixed-layer results. The fact that $R = 1.55$ in the lower mixed layer is a reflection of the larger value of B (1.30 rather than 0.85) required to fit the data in Fig. 9b.

Frisch and Ochs (1975) have defined a dimensionless temperature structure function parameter for the mixed layer based on Equation 7b:

$$G(Z/Z_i) = C_T^2/3.2\, B\theta_*^2 Z_i^{-2/3}(Z/Z_i)^{-4/3}. \tag{15}$$

In Fig. 11 the Panama City data are compared with the over-water data of Frisch and Ochs (1975) and the over-land data of Kaimal *et al.* (1976).

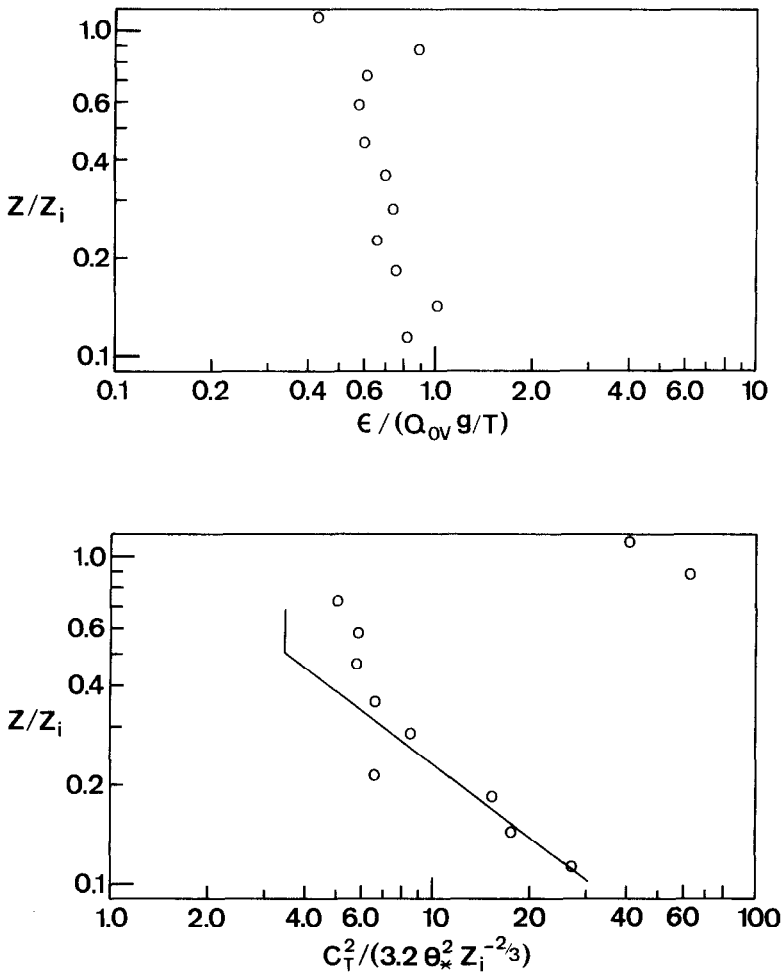

Fig. 9. Average profile of dimensionless turbulence quantities in mixed layer scaling (Equation 14). (a) Rate of dissipation of turbulent kinetic energy (b) Temperature structure function parameter. The solid line is a reproduction of the overland results of Kaimal *et al.* (1976) with $B = 1.30$.

9. Discussion

The results for ε agree with the empirical formula of Wyngaard *et al.* (1971a) from the near surface to $Z/Z_i = 0.8$. The C_T^2 results require discussion. In Fig. 5b we can see considerable deviations of the C_T^2 from the surface-layer scaling formula (Equation 5a). The fact that the data lie on the expected curve for $-Z/L \ll 1$ is not significant since the values of T_* were selected to force a fit in this region. In the lower mixed layer ($0.1\ Z_i < Z < 0.4\ Z_i$), where C_T^2 is relatively uninfluenced by the inversion, we expect compatibility between the surface- and mixed-layer C_T^2 profiles. Since the lower mixed-layer C_T^2 data (Fig. 10) are about 55% higher than expected, we conclude that the near surface ($Z < 30$ m) C_T^2 values are in basic disagreement with

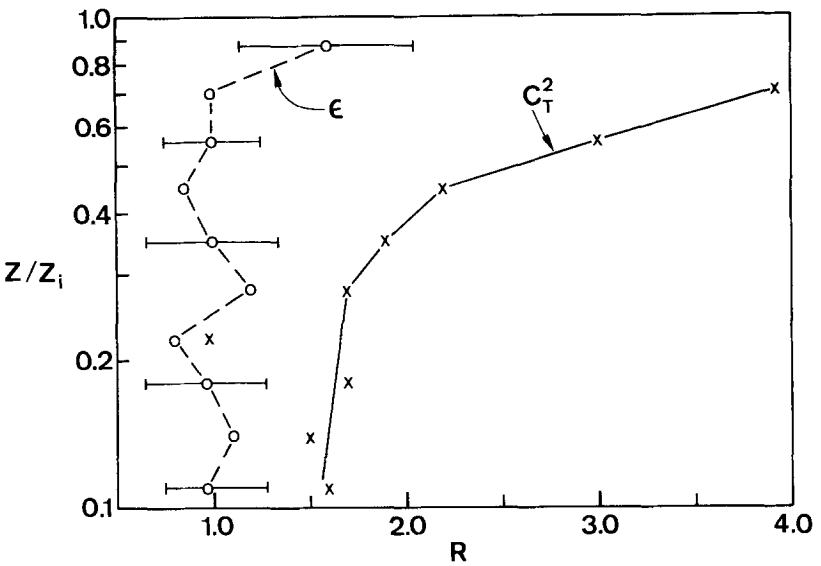

Fig. 10. Average of R (Equation 13) in the mixed layer. The horizontal bars show typical uncertainties in the mean estimate.

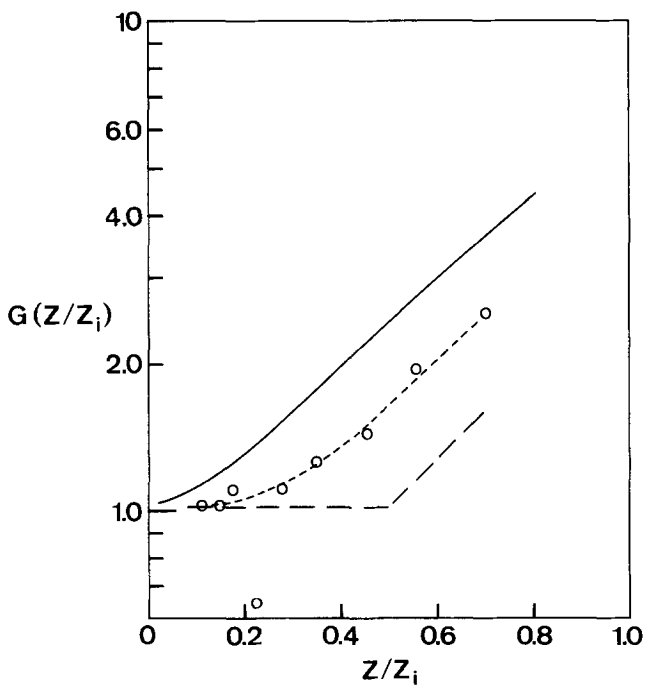

Fig. 11. The average mixed layer dimensionless temperature structure function parameter (Equation 15). The solid line is from Frisch and Ochs (1975) where $\bar{Z}_i$ = 300 m. The dotted line and circles is the Panama City data where $\bar{Z}_i$ = 700 m. The dashed line is from Kaimal *et al.* (1976) where $\bar{Z}_i$ = 1700 m.

those from the lower mixed layer. It is of interest to speculate on the possible significance of this. Recall that Equation 5a was based on over-land measurements (Wyngaard *et al.*, 1971b) with only a few points for $-Z/L > 1$. However, the more recent mixed-layer C_T^2 measurements of Kaimal *et al.* (1976) were compared with the convective limit of Equation 9b and excellent agreement was found for $0.1\, Z_i < Z < 0.5\, Z_i$. Thus, one can have confidence in Equation 5a for the over-land case. The over-water measurements of Davidson *et al.* (1979) show disagreement with Equation 5a similar to that of Fig. 5b but this disagreement is attributed to probable sea-salt contamination of the sensors. Although we initially rejected the hypothesis of an altitude measurement error because of our success with the ε data, the greater height dependence of R_T at lower altitudes (Fig. 6) does imply that the discrepancy is some type of surface effect. It is conceivable that, in fact, the altitude measurement is in error and *both* C_T^2 and ε depart from the over-land results near the surface. Recall that in Section 3 the isotropy effect on the C_T^2 measurement process was estimated to have an upper limit of 10% at $Z = 3$ m (Fig. 1a). The probe spacing comparison shown in Fig. 1b indicates the effect is slightly greater with narrower probe spacing. This suggests a frequency response or noise drift problem with the measurements. Neither of these effects is very large and it is not clear that they would be height-dependent. Furthermore, we have discovered that this effect is not unique to temperature measurements but has also been observed in microwave C_N^2 data recently acquired in the Bahamas. Certainly this does not preclude the possibility of some other measurement error but no such effects have been discovered as yet. Since we are unable to propose a physical mechanism for this discrepancy, we prefer to leave it as an interesting unexplained result.

Even without a resolution of the surface-layer disagreements, the mixed-layer results shown in Fig. 11 are significant. They strongly suggest that the mixed-layer dimensionless temperature structure function, $G(Z/Z_i)$, is not a 'universal' similarity function. It is likely that $G(Z/Z_i)$ is influenced by Z_i (note that different values of $\bar{Z}_i$ for the three sets of data) or the temperature discontinuity at the inversion.

References

Businger, J. A.: 1973, 'Turbulent Transfer in the Atmospheric Surface Layer', *Workshop on Micrometeorology*, (D. Haugen, Ed.) American Meteorological Society, 67–98.

Davidson, K. L., Houlihan, T. M., Fairall, C. W., and Schacher, G. E.: 1978, 'Observations of the Temperature Structure Function Parameter, C_T^2, Over the Ocean', *Boundary-Layer Meteorol.* **15**, 507–523.

Fairall, C. W. and Markson, R.: 1979, 'Aircraft Measurements of Micro-meteorological Parameters at Panama City, Florida in 1978', Nav. Postgrad. Sch. Technical Report. Copies can be obtained by writing to the Authors or to the Defense Documentation Center.

Frisch, A. S. and Ochs, G. R.: 1975, 'A Note on the Behavior of the Temperature Structure Parameter in a Convective Layer Capped by a Marine Inversion', *J. Appl. Meteorol.* **14**, 415–419.

Kaimal, J. C., Wyngaard, J. C., Izumi, Y., and Cote, O. R.: 1972, 'Spectral Characteristics of Surface Layer Turbulence', *Quart. J. Roy. Meteorol. Soc.* **98**, 563–589.

Kaimal, J. C., Wyngaard, J. C., Haugen, D. A., Cote, O. R., and Izumi, Y.: 1976, 'Turbulence Structure in the Convective Boundary Layer', *J. Atmos. Sci.* **33**, 2152–2169.

LeMone, M. A.: 1973, 'The Structure and Dynamics of Horizontal Roll Vortices in the Planetary Boundary Layer', *J. Atmos. Sci.* **30**, 1077–1091.

Lenschow, D. H.: 1974, 'Model of the Height Variation of the Turbulence Kinetic Energy Budget in the Unstable Planetary Boundary Layer', *J. Atmos. Sci.* **31**, 465–474.

Panofsky, H. A.: 1978, 'Matching in the Convective Planetary Boundary Layer', *J. Atmos. Sci.* **35**, 272–276.

Wyngaard, J. C., Cote, O. R., and Izumi, Y.: 1971a, 'Local Free Convection, Similarity, and the Budgets of Shear Stress and Heat Flux', *J. Atmos. Sci.* **28**, 1171–1182.

Wyngaard, J. C., Izumi, Y., and Collins, S. A.: 1971b, 'Behavior of the Refractive Index Structure Parameter near the Ground', *J. Opt. Soc. Am.* **61**, 1646–1650.

Wyngaard, J. C., Pennell, W. T., Lenschow, D. H., and LeMone, M. A.: 1978, 'The Temperature-Humidity Covariance Budget in the Convective Boundary Layer', *J. Atmos. Sci.* **35**, 47–58.